

- [8] G. Cerri, R. D. Leo, and V. M. Primiani, "Theoretical and experimental evaluation of the electromagnetic radiation from apertures in shielded enclosures," *IEEE Trans. Electromagn. Compat.*, vol. 34, no. 4, pp. 423–432, Nov. 1992.
- [9] M. P. Robinson, T. Benson, C. Christopoulos, J. F. Dawson, M. D. Ganley, A. C. Marvin, S. J. Porter, and D. W. P. Thomas, "Analytical formulation for the shielding effectiveness of enclosures with apertures," *IEEE Trans. Electromagn. Compat.*, vol. 40, no. 3, pp. 240–248, Aug. 1988.
- [10] R. Azaro, S. Caorsi, M. Donelli, and G. L. Gragnani, "A circuitual approach to evaluating the electromagnetic field on rectangular apertures backed by rectangular cavities," *IEEE Trans. Microw. Theory Tech.*, vol. 50, no. 10, pp. 2259–2266, Oct. 2002.
- [11] Z. A. Khan, C. F. Bunting, and M. D. Deshpande, "Shielding effectiveness of metallic enclosures at oblique and arbitrary polarizations," *IEEE Trans. Electromagn. Compat.*, vol. 47, no. 1, pp. 112–122, Feb. 2005.
- [12] T. Yang and J. L. Volakis, "Coupling onto wires enclosed in cavities with apertures," *Electromagnetics*, vol. 25, no. 7/8, pp. 655–678, 2005.
- [13] A. E. Ruehli, "Equivalent circuit models for three-dimensional multi-conductor systems," *IEEE Trans. Microw. Theory Tech.*, vol. 22, no. 3, pp. 216–221, Mar. 1974.
- [14] Y. Bayram and J. L. Volakis, "Hybrid s-parameters for transmission line networks with linear/nonlinear load terminations subject to arbitrary excitations," *IEEE Trans. Microw. Theory Tech.*, vol. 55, no. 5, pp. 941–950, May 2007.
- [15] Y. Hua and T. K. Sarkar, "Generalized pencil-of-function method for extracting poles of an EM system from its transient response," *IEEE Trans. Antennas Propag.*, vol. 37, no. 2, pp. 219–234, Feb. 1989.

## Measurement and Modeling of the Magnetic Near Field Radiated by a Buck Chopper

Ouafae Aouine, Cécile Labarre, and François Costa, *Member, IEEE*

**Abstract**—Static converters are used with increasingly high switching frequencies. Consequently, they impose increasingly severe electromagnetic interference (EMI) constraints in their environment. In order to study and to quantify the radiated perturbations, we have used a test bench for measuring the magnetic field radiated in the near zone. In this paper, we present measurements of the magnetic field radiated by the switching cell of a Buck chopper in the near field at high and low frequencies. By comparing the mappings of the magnetic field over the switching cell with the ones of a circular loop, we have deduced that the switching cell can be effectively modeled by a loop. The loop's geometric characteristics and its equivalent current flowing in have been determined from near magnetic field data. The model has been validated at high and low frequencies.

**Index Terms**—Magnetic field measurement, near field, power electronics.

### I. INTRODUCTION

Power electronics are used for energy conversion in many applications such as automotive, aeronautics, or household appliances. The

Manuscript received August 28, 2007; revised November 16, 2007.

O. Aouine is with the Department of Informatique and Automatique (IA), Ecole des Mines de Douai, 59508 Douai, France, and also with Schneider Electric Company, 38050 Grenoble, France (e-mail: aouine@ensm-douai.fr).

C. Labarre is with the Department of Informatique and Automatique (IA), Ecole des Mines de Douai, 59508 Douai, France (e-mail: labarre@ensm-douai.fr).

F. Costa is with the SATIE (UMR 8029), ENS de Cachan PRES UniverSud, 94230 Cachan, France, and also with the IUFM de Créteil, Université Paris 12, 93000 Saint Denis, France (e-mail: francois.costa@satie.ens-cachan.fr).

Color versions of one or more of the figures in this paper are available online at <http://ieeexplore.ieee.org>.

Digital Object Identifier 10.1109/TEMC.2008.922794

magnetic fields they generate may disturb nearby circuits. Moreover, the variations of currents and voltages in converters are very fast and their amplitudes are great, which causes very high electromagnetic disturbances over a large range of frequencies. The aim of this research is to measure the magnetic near field radiated by a typical converter, using a test bench that achieves a mapping of the radiated near field, in order to locate and to model the near-zone radiating sources.

Section II will depict the test bench for mapping [1]. The near-field scanner measures the magnitude of the magnetic field over a ground plane at a specific height above the power converter. Thanks to this equipment, it is possible to locate the switching cell in the converter, usually constituted by the circuit delimited by the decoupling input capacitor, a diode and a power switch. Actually, in this circuit, the current and voltage exhibit high-level transients ( $dV_{DS}/dt$ ,  $dI_{DS}/dt$ ); outside of it, these quantities are quite constant, showing a low-level ripple. This will be described in Section II (see representation in Fig. 1). In Section III, we will present the measurement results of the near-field scanning. A previous study has shown that the switching cell could be modeled by a circular loop, whose geometrical and electrical characteristics can be deduced from the near-field mapping [2]. Section IV will recall these aspects.

We have adopted the following methodology. At first, a spectral analysis of the magnetic near field radiated locally over the converter is conducted. The maximal amplitude peak frequencies are identified. Next, a near-field mapping is done for each of these frequencies at a defined height above the converter. Thanks to this, the equivalent sources are identified.

## II. EXPERIMENTAL SETUP

### A. Test Bench

The test bench consists of a near-field magnetic probe, a ground plane (60 cm × 50 cm), a 2-D displacement table, and an electromagnetic interference (EMI) receiver (9 kHz to 2.9 GHz): the probe is connected to the EMI receiver and is mounted on a two-axis displacement table. A computer monitors the probe displacement (along  $X$  and  $Y$ ) over the converter and records data provided by the EMI receiver [3]–[5]. The displacements along the  $X$ - and  $Y$ -axes have been chosen to be close to 50 cm.

The heat sink (usually large) cooling a power converter acts as a ground plane for electronics. This is the reason why we have chosen to insert a copper ground plane on the displacement table in order to take into account this characteristic of power electronics. All the displacement devices (motors, electronic drivers), which are likely to induce electromagnetic perturbations, are located under the ground plane. All the structural parts, which stand above this area, are made of unreflecting materials (plexiglas, nylon).

We used magnetic probes with a negligible radius (5 mm) as compared to the wavelength of the interfering signal. These probes average the magnetic field strength in the loop area of the probe head. Their frequency range is 10 kHz to 50 MHz or 30 MHz to 3 GHz. They have been calibrated with a TEM cell in order to determine their antenna factor. Results are presented in the form of mappings of the magnetic near field radiated, the EMI receiver giving rms values, expressed in decibels per microampere per meter ( $\text{dB}\cdot\mu\text{A}/\text{m}$ ).

### B. Converter Under Test

Fig. 1 shows a picture of the studied converter. The buck chopper is fed by a 50-V voltage source  $E$ ; its switching frequency is  $f_s = 20$  kHz. It provides a 2-A current  $I_o$  in the output resistive load when the duty cycle is 0.5. The control signal is transmitted to the MOSFET,

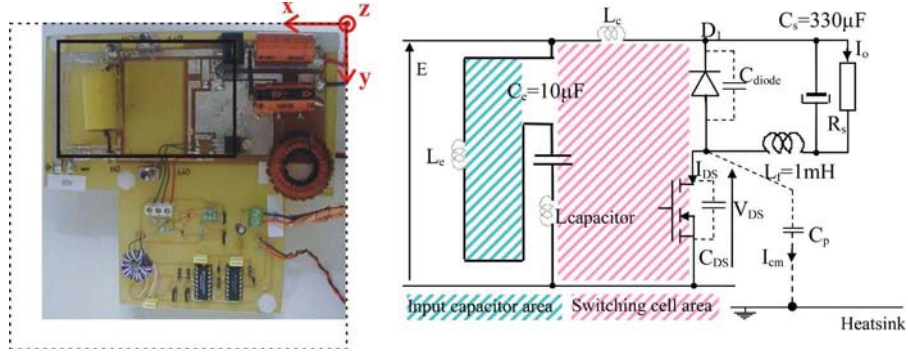


Fig. 1. Picture and electric diagram of the converter; solid line rectangle: the switching cell; dashed line square: the scan area.

thanks to a highly insulated driver, avoiding disturbances to propagate through this circuit. Moreover, it has negligible influence to the power part. Near-field measurements have been done previously over the control circuit that has shown its little influence as compared to one of the power circuit. Actually, the converter is not designed with respect to industrial standards; however, it will enable us to locate and quantify the radiating sources and to link their effect with a well-known quantity such as the parasitic inductance of the circuit. Moreover, the effect of magnetic components supplied by high-level high-frequency (HF) currents (transformer, resonant inductors) has not been studied. A similar methodology could be applied in any industrial device.

The parasitic elements that contribute significantly to the disturbances (radiated and conducted) are represented in the electric diagram of the converter (see Fig. 1). The two parasitic inductances  $L_e$  (intrinsic inductance of the input capacitor) and  $L_c$  (inherent inductance of the switching cell) have a great influence on the radiated magnetic field; they are proportional to the radiating areas of the converter (hatched areas). Moreover, the current  $I_{DS}$  in the switching cell, itself being determined by the output load current  $I_o$ , is another important parameter for the radiation of the converter. The parasitic capacitance  $C_p$  determines the common mode current  $I_{cm}$ . It has a value sufficiently small not to influence the main phenomena due to the switching cell.

### III. NEAR-FIELD MEASUREMENTS

#### A. Identification of the Maximal Radiation Frequencies

We have measured the  $z$ -component of the radiated magnetic field at an 8-cm height above the converter at the middle of the switching cell in two frequency bands (according to the probes frequency range): 9–350 kHz and 350 kHz to 300 MHz, with an intermediate frequency (IF) bandwidth, respectively, equal to 200 Hz and 9 kHz. The corresponding spectrum is represented on Fig. 2. The gap observed at 350 kHz is due to the IF bandwidth change.

At low frequencies, we can identify the switching frequency and its harmonics. The maximum level is obtained for the fundamental (20 kHz), and the level of emission of the even harmonics is higher than for the odd harmonics, due to the duty cycle close to 0.5. At high frequencies, we notice that the maximum radiation level is obtained at frequency  $f_1 = 17.9$  MHz. This frequency corresponds to the resonance between the intrinsic capacitances of the semiconductors ( $C_{DS}$  or  $C_{diode}$ ) when one of them is switched off, with the parasitic inductances of the switching cell.

This phenomenon can be easily observed in the MOSFET current  $I_{DS}$  at switching ON and OFF, as shown in Fig. 3. We can notice HF parasitic oscillations on the waveforms; they correspond quite exactly to the peaks of the HF spectrum. The ringing frequency on  $I_{DS}$  at

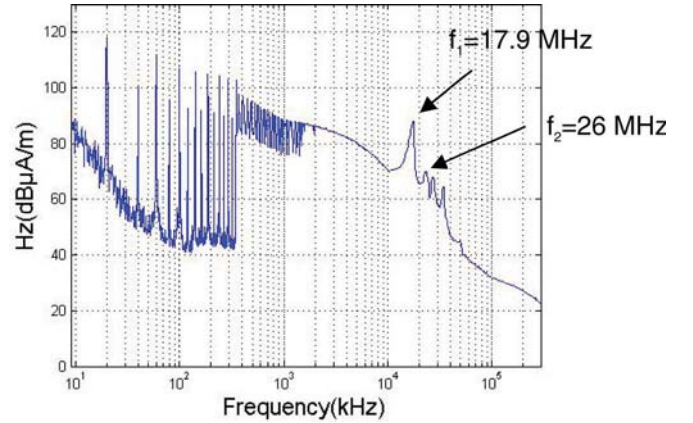


Fig. 2. Amplitude of the  $z$ -component of the magnetic near field (LF part: 9 kHz to 300 MHz).

switching OFF is equal to  $f_1 = 17.9$  MHz, and it is equal to 26 MHz at switching ON.

By using the circuit represented in Fig. 1 and supposing that the MOSFET and diode can be considered as ideal switches, the current  $I_{DS}$  at switching OFF can be expressed by

$$I_{DS} = E \sqrt{\frac{C_{DS}}{L_T}} [\sin(\omega_{HF} t) + \zeta \cos(\omega_{HF} t)] \exp(-\zeta \omega_{HF} t) \quad (1)$$

where  $C_{DS}$  is the drain-to-source capacitance,  $L_T$  is the total parasitic inductance of the switching cell (see Section IV-A for its measurement), the ringing frequency (switching OFF)  $\omega_{HF-OFF} = 1/\sqrt{L_T C_{DS}}$ , and  $\zeta$  is the damping factor of the ringing, due to losses in the switching cell.

The same kind of ringing occurs at switching ON involving the same parasitic inductance with the diode intrinsic capacitance  $C_{diode}$ . The current  $I_{DS}$  expression is identical as in (1), replacing  $C_{DS}$  by  $C_{diode}$  and the ringing frequency is:  $\omega_{HF-ON} = 1/\sqrt{L_T C_{diode}}$ , that is, 26 MHz.

Moreover, other high-frequency ringings that can be observed on the HF spectrum are due to other smaller capacitive effects (distributed capacitance of the output inductance, printed circuit board (PCB) to ground capacitance, etc.). They are not considered herein because they have second-order effects on the current waveforms. In conclusion, we can say that the magnetic field emission at high frequencies (far from the switching frequency) is mainly caused by the  $dI/dt$  and  $dV/dt$  during the switching transients of the transistor: they excite the ringing modes of the switching cell, leading to a high-frequency current as presented before.

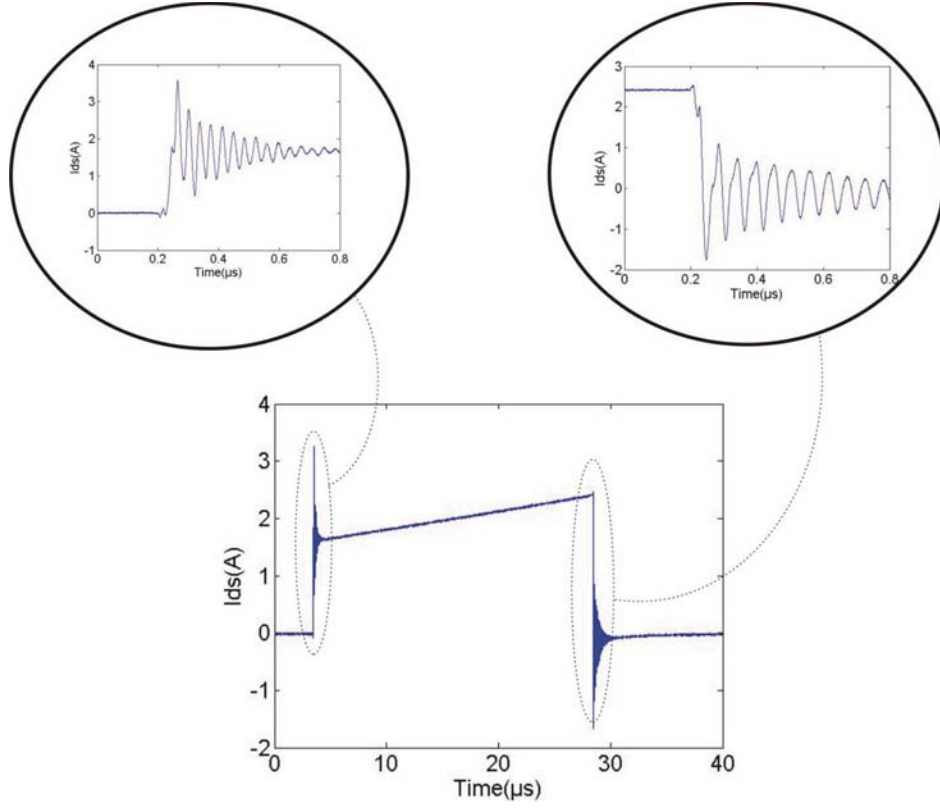


Fig. 3. Current  $I_{DS}$  waveform, switching ON and OFF.

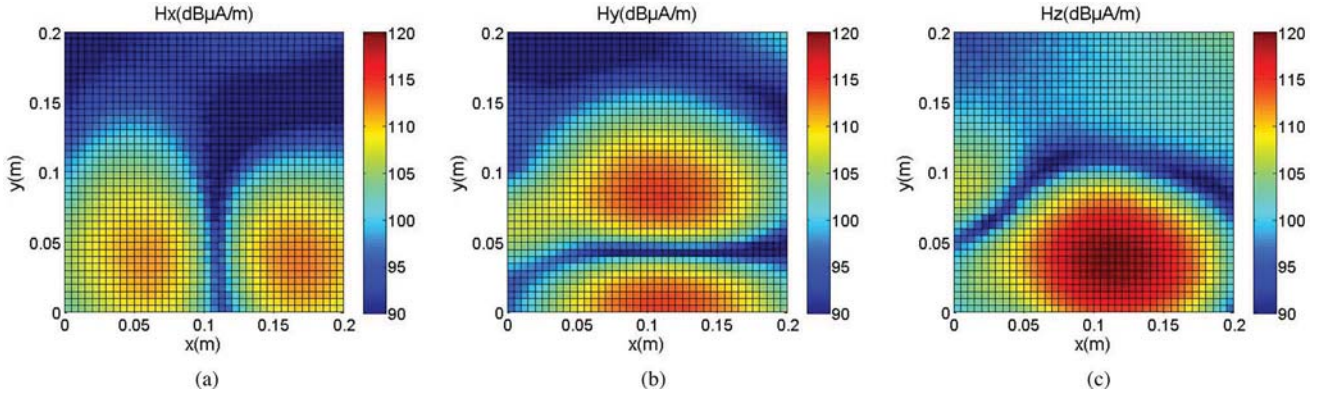


Fig. 4. Measured magnetic near field,  $f = 20$  kHz. (a)  $x$ -component. (b)  $y$ -component. (c)  $z$ -component.

In order to investigate the near-field perturbing modes of the converter, we have selected two frequencies: the switching frequency (20 kHz), which generates a strong magnetic field over the switching cell, and one at high frequency (17.9 MHz) for which the radiated field amplitude is maximal, as can be seen in the spectrum (see Fig. 2). In the following part, we perform a near-field scanning above the converter at these frequencies.

### B. Low-Frequency Measurement

We have measured the magnetic field above the converter at a height of 8 cm above the converter. The scan area is  $20 \text{ cm} \times 20 \text{ cm}$ , and it is represented in Fig. 1 by a dashed line square. We have represented in Fig. 4 the three components of the measured magnetic field at 20 kHz, the switching frequency.

These measurements show the following.

- 1) The mapping of the radiation of the converter is close to the one of a current loop [1].
- 2) The  $z$ -component is the most important one. The noise level on the  $H_z$  component is much higher ( $100 \text{ dB} \cdot \mu\text{A/m}$ ) than the two other components  $H_x$  and  $H_y$  ( $90 \text{ dB} \cdot \mu\text{A/m}$ ).
- 3) The control board produces a negligible magnetic field (as previously told). The power circuit creates a significant magnetic field centered on the switching cell constituted by the MOS transistor, the diode, and the decoupling capacitor  $C_e$  (solid line rectangle in Fig. 1). The field radiated by the output inductor appears on the  $z$ -component of the magnetic field; its level is much lower than the one radiated by the switching cell.
- 4) The maximum field value is located at the center of the switching cell ( $120 \text{ dB} \cdot \mu\text{A/m}$ ).

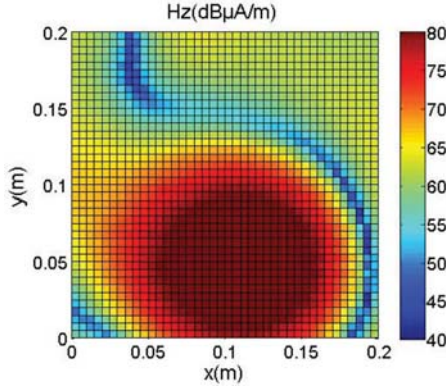


Fig. 5. Measured magnetic near-field  $z$ -component,  $f = 17.9$  MHz.

### C. High-Frequency Measurement

For the same height and for the same scan area, we have also measured the three components of the magnetic field at 17.9 MHz. We obtained the following result, shown in Fig. 5. Hereafter, we have chosen to represent only the  $z$ -component, the most important component of the magnetic field because the discussions about the  $y$ - and  $x$ -components are the same as for the  $y$ - and  $x$ -components of the previous measurements.

It is interesting to note that the radiating patterns are nearly identical at low and at high frequencies, the electrical circuits involved and the areas concerned being the same. So, a single model can be proposed for both, low- and high-frequency near-field predictions, as we will propose next.

## IV. EQUIVALENT SOURCE DETERMINATION

### A. Modeling in Low Frequency

From the mappings in Figs. 4 and 5, we can notice that they are very similar to the ones of an ordinary circular loop [6], [7]. We have searched the characteristics of an equivalent loop (center position, diameter, and current) parallel to the ground plane in order to model the switching cell in this way.

The center of the loop is determined by the position where the amplitude of  $H_z$  is maximal and is equal to  $H_c$ . To determine the radius of the equivalent loop, we have measured the distance between the minimum and the maximum of the amplitude of the component  $H_x$  (or  $H_y$ ). From the formula for the magnetic field radiated by a loop above a ground plane [1], [2] expressed by (2), we can calculate the equivalent sinusoidal current  $I_{eq}$ , which flows in the equivalent loop.

$$H_c = \frac{I_{eq} a^2}{2} \left[ \frac{1}{((z-h)^2 + a^2)^{3/2}} - \frac{1}{((z+h)^2 + a^2)^{3/2}} \right] \quad (2)$$

where  $a$  is the loop radius,  $h$  is the loop height above the ground plane,  $z$  is the probe height above the ground plane, and  $H_c$  is the amplitude of the magnetic field in the center of the loop.

In the measurement conditions corresponding to the mapping of Fig. 4, we have found the following parameters of an equivalent loop: its radius  $a$  is equal to 4 cm and the rms value of the sine wave current  $I_{eq}$  is equal to 0.95 A. This is in good agreement with the real current  $I_{DS}$  of the switching loop (see Fig. 3) whose fundamental is close to 1.3 A. (We recall that the switching frequency is 20 kHz, the loop is in the same plane as the converter, i.e.,  $h = 4$  cm above the ground plane, and the measurement is performed at a height  $z$  equal to 12 cm.)

Using these parameters, we have simulated the three components of the magnetic field radiated by the equivalent loop. We have only represented the  $z$ -component in Fig. 6. Some agreements and differences can be observed: the center of the radiating area is correctly identified, the field amplitude at this point too, and the pattern of the calculated field is perfectly circular, that is not the case for the measurements. This is due to the fact that the radiating area is close to a rectangle and the model is a circular one. Moreover, the radiating loop is not perfectly parallel to the ground plane; the input capacitor of the converter is situated in a vertical plane relative to the printed board; it behaves like a vertical loop whose effect is combined with the one of the switching cell, leading to an additional  $y$ -component to the radiated field. At last, the radiation of the output inductance (see in Fig. 1) can be observed by the yellow mark at  $x = 0, y = 0.1$ .

### B. Calculation of the Total Parasitic Inductance of the Switching Cell

Moreover, the mapping can be used to determine the parasitic inductance of the switching loop, as presented next. The magnetic flux issued from the switching cell area  $S$  of the chopper is equal to:

$$\Phi = \iint_{(S)} \vec{B} \cdot \vec{dS} \quad (3)$$

For the first harmonic of the switching frequency (at 20 kHz), this parasitic flux can also be considered as the consequence of the current  $I_{eq}$  flowing in the total parasitic inductance of the switching cell, thus,

$$\Phi = L_T I_{eq} \quad (4)$$

where  $\vec{B}$  is the magnetic field radiated in near field,  $S$  is the switching cell area,  $L_T$  is the total parasitic inductance of the circuit, and  $I_{eq}$  is the equivalent sine current flowing in the circuit (at 20 kHz, i.e., the fundamental of the real current  $I_{DS}$ ).

So, using the mapping and the equivalent loop model, it is easy to calculate the flux issued from the area of the equivalent loop, and knowing the current  $I_{eq}$  to determine the parasitic inductance of the switching cell from (4). We have found  $L_T = 423$  nH, which corresponds to the sum of  $L_e$  and  $L_c$ . A direct measurement using a network analyzer gave  $L_e + L_c = 475$  nH. The values are in a good agreement. So, this method is valuable in order to measure the parasitic inductance when the direct measurement cannot be employed. In our case, the reduction of the parasitic inductance means a reduction of the radiated field.

### C. Modeling in High Frequency

In this section, we will show that the same model of a radiating loop can be used for the HF prediction of the radiated magnetic near field. Using the same geometrical parameters for the equivalent loop (Section IV) and an equivalent current of  $I_{eq, HF} = 20$  mA at 17.9 MHz in the equivalent loop, we have calculated the  $z$ -component of the magnetic field and compared it to the measurement, as represented in Fig. 7. The two figures match quite well for  $x > 0.1$ . For  $x < 0.1$ , we can see the effect of the output inductance magnetic field like for the lower frequency [see in Fig. 6(b)]. The two magnetic fields are merging together. This explains why the  $H_z$  measurement mapping seems to be asymmetric contrary to the simulation, which does not include the output inductance effect. This does not question the validity of the modeling principle.

By comparing these mappings to the ones of Fig. 6, we can conclude that the modeling of the switching cell by a loop is also valid at high frequencies; this is due to the fact that the parasitic ringings occur in the same geometrical circuit where the power is converted (i.e., the switching cell).

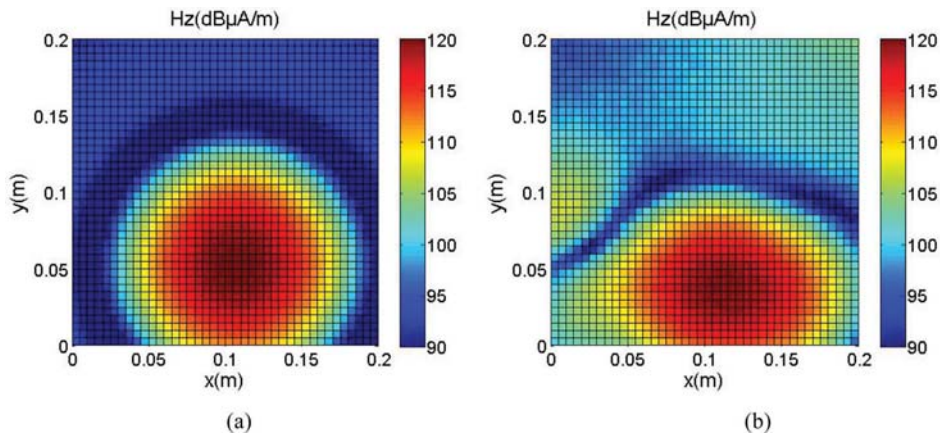


Fig. 6. Magnetic near-field  $z$ -component,  $f = 20$  kHz. (a) Simulated. (b) Measured.

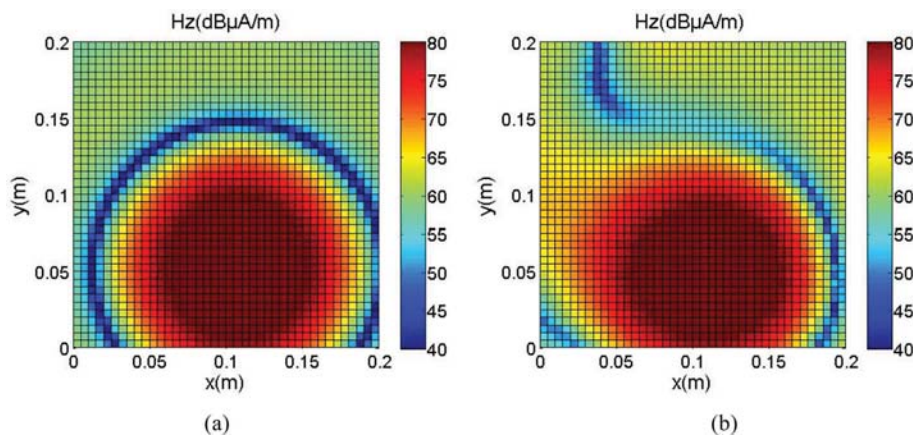


Fig. 7. Magnetic near-field  $z$ -component at high frequency. (a) Simulated. (b) Measured.

## V. CONCLUSION AND PERSPECTIVES

The approach presented in this paper gives an experimental method for identifying EMI sources and for modeling them by equivalent sources at low and high frequencies. As an example, we have measured the EMI radiated by a buck chopper in the near field. Consequently, we can model a switching cell by a circular magnetic dipole whose geometrical characteristics and equivalent current are given from the magnetic field measured in the near field. We can use this approach to model other sources of radiation inside different power electronic systems.

The next step will be to use the same bench to evaluate the radiation of more complex systems in order to identify the various disturbing sources to compare their levels of emission with the standards, and to study the various possibilities to decrease the radiation and to avoid couplings between “hot” sources (switching cells, magnetic components) and sensitive components (filter).

## REFERENCES

- [1] E. Béreau, C. Labarre, and F. Costa, “Measurement bench for electromagnetic near field characterization of power electronics devices,” presented at the Symp. Embedded EMC, 2EMC, Rouen, France, 2005.
- [2] B. Essakhi, D. Baudry, O. Maurice, A. Louis, L. Pichon, and B. Mazari, “Characterization of radiated emissions from power electronic devices: Synthesis of an equivalent model from near-field measurement,” *Eur. Phys. J.—Appl. Phys.*, vol. 38, no. 3, pp. 275–281, Jun. 2007.
- [3] D. Baudry, A. Louis, and B. Mazari, “Characterization of the open-ended coaxial probe used for near-field measurements in EMC applications,” *Progress Electromagn. Res.*, vol. 60, pp. 311–333, 2006.
- [4] D. Baudry, F. Birel, L. Bouchelouk, A. Louis, B. Mazari, and P. Eudeline, “Near-field techniques for detecting EMI sources,” in *Proc. IEEE Int. Symp. Electromagn. Compat.*, 2004, vol. 1, pp. 11–13.
- [5] F. D. Daran, J. Chollet-Ricard, F. Lafon, and O. Maurice, “Prediction of the field radiated at one meter from PCB’s and microprocessors from near EM field cartography,” in *Proc. IEEE Int. Symp. Electromagn. Compat., EMC’03*, 2003, pp. 479–482.
- [6] C. A. Balanis, *Antenna Theory—Analysis and Design*, 2nd ed. New York: Wiley, 1997.
- [7] G. S. Smith, *An Introduction to Classical Electromagnetic Radiation*. Cambridge, U.K.: Cambridge Univ. Press, 1997.